ACS OMEGA

http://pubs.acs.org/journal/acsodf

Article

Optimum Strategy for Perforating Distribution of Homogeneous Gas−Liquid Two-Phase Flow in Vertical Gas Wells

Jiancheng Hu*

Cite This: *ACS Omega* 2021, 6, 13066−13076

Read Online

ACCESS | Metrics & More | Article Recommendations

ABSTRACT: Aiming to optimize the total production of homogeneous gas−liquid two-phase flow in perforated vertical gas wells, a new coupled reservoir−wellbore mathematical model is proposed which consists of the crushed zone damage skin factor, pressure gradient, flow rate, and liquid holdup. An optimum strategy consisting of two optimization problems is developed to study the effect of perforation distribution on the production of vertical wells under a steady-state inflow. Then, these optimization models are applied to infinite and finite conductivity gas wells and the optimal distribution of perforation could be determined. The results show that inflow rate profiles could be improved by optimizing the perforation location for vertical gas wells.

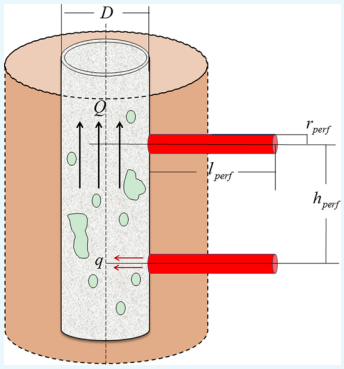

1. INTRODUCTION

In the petrochemical industry, multiphase flow in pipelines is a common phenomenon, especially for gas−liquid two-phase flow. Because the two-phase flow is no less complex than the single-phase turbulent flow, it is quite difficult to obtain the theoretical solution of the two-phase flow. In the case of perforation completion, reservoir fluids are connected with a wellbore through perforation. In order to predict the productivity of perforation completion, some factors affecting the fluidity near the wellbore should be considered. The flow pattern, the pressure gradient, the mass transfer between two phases, liquid holdup, distribution of the hole, and the degree of damage to the formation caused by the perforation process, and so forth have a great influence on the determination of productivity. Because of the complexity of the two-phase flow in the pipe, the productivity of perforation completion is much more difficult than that of open-hole wells. Since the late 1980s, many researchers have tried to utilize empirical or semiempirical methods to develop prediction techniques.[1−10]

Kissling et al. studied the vertical single-component two-phase flow in porous media under the action of gravity and found that two phases could simultaneously flow in opposite directions, depending on the sign of fluid velocity.[11] The drift flux model was used in the calculation of liquid holdups and has been widely applied in models of the multiphase flow in pipelines. However, previous studies have indicated that these models are confined to a group of fluid properties, pipeline geometry, and operating conditions. Choi et al. proposed a new closed relation of the drift flux to simulate the liquid holdup in pipelines, which is suitable for various flow conditions.[12] Based on previous models, a mechanical model of the gas−liquid two-phase flow in vertical pipelines is improved, which can predict the flow pattern conversion, pressure gradient, gas holdup, liquid holdup, and slug characteristics of the gas−liquid two-phase flow in vertical pipelines.[13] A high rate of oil and gas flow has a positive effect on the fluid flowing through the pipelines' structure between the casing and tubing. Liu et al. improved the distribution coefficient and the drift velocity of drift flow models for horizontal and upward inclined gas−liquid two-phase flow.[14] A large number of literature studies have been reported on the mechanism of gas−liquid two-phase flow in a gas pipeline.[9,15−21]

In the exploration and production of oil and gas, perforation completion is one of the most widely used completion methods. The initial stage of gas well exploitation is anhydrous gas production, and the gas flow is single phase in the wellbore.

The gas−liquid two-phase flow occurs in the wellbore when the formation water intrudes into the bottom of the wellbore. When the gas production is greater than the unload flow, the gas well is in the stage of gas production with water. Many researchers have studied the effects of the reservoir, wellbore, and perforation parameters on the productivity of perforated wells. Islam and Chakma proposed a model which can describe the inflow through perforations into a two-phase flow within the

Received: February 9, 2021
Accepted: April 29, 2021
Published: May 12, 2021

https://doi.org/10.1021/acsomega.1c00748
ACS Omega 2021, 6, 13066−13076

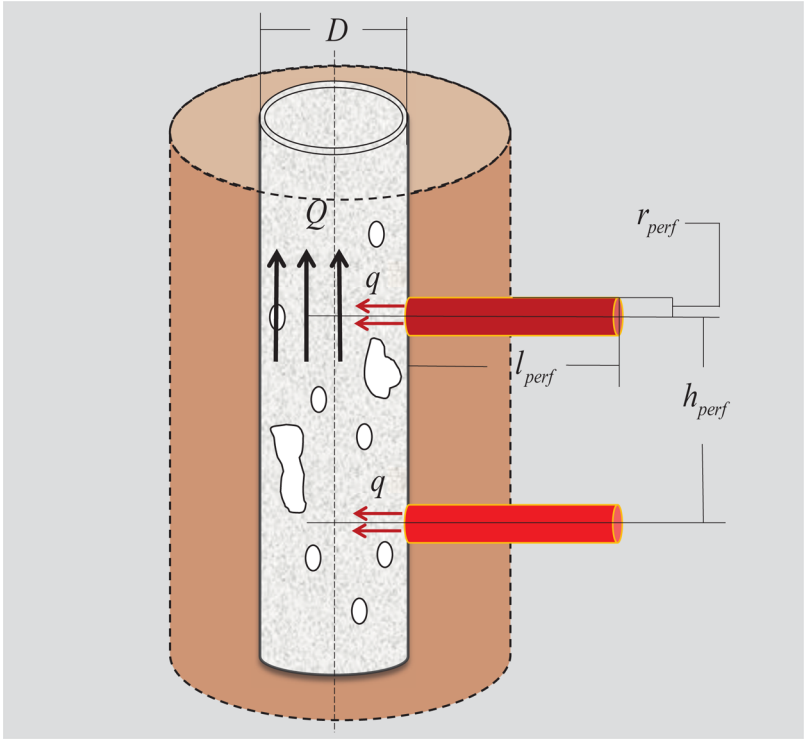

Figure 1. Vertical array of perforations.

wellbore, but the model did not investigate the impact of perforation distribution.[22] Landman and Goldthorpe first presented a model which couples the Darcy flow and inflow from the perforation for the horizontal well flow and studied how perforation distribution affects the well production.[23] Later, numerous research works also studied the main factors, such as steady flow, heterogeneous reservoir, skin factor, flow efficiency, water or gas coning, and so forth, on how to influence inflow profiles in vertical single- or multiphase gas wells.[10,14,24−30] However, the optimization of the perforating parameter for two-phase vertical wellbores has not been further studied in petroleum production engineering.

A simplified coupled model of the two-phase flow in a vertical perforated wellbore is established in this paper. Perforation distribution, pressure gradient of a wellbore, liquid holdup, and flow rate are considered in the coupled reservoir-wellbore model. Besides, two optimization models are presented to describe the effect of perforation parameters on well productivity, and some examples of numerical predictions are illustrated based on a vertical gas−liquid well.

2. MODELING

2.1. Reservoir Model of Perforation Wells. Perforations are considered to be cylinder shaped and gas and liquid two-phase fluid flow through the perforations from the reservoir or porous media into the wellbore, as shown in Figure 1.

For simplicity, it is assumed that formation damage is negligible. Assuming perforation i is positioned at $z = z_i$, which is unknown variables related to perforation density. The total pressure p_i of hole i consists of two parts: self-induced pressure p_{ii} due to its own inflow and pressure p_{ij} $(i \neq j)$due to the inflow from all other holes[31]

$$p_i = p_{ii} + \sum_{j \neq i} p_{ij} \tag{1}$$

The pressure of perforation i induced by the inflow $q_{\mathrm{Im},i}$ of itself is defined by

$$p_{ii} = -\frac{\mu}{4\pi k}\frac{q_{\mathrm{Im},i}}{r_{\mathrm{peq}}} \tag{2}$$

in which q_{Im} is the volume inflow rate of the mixture unit perforation depth

$$q_{\mathrm{Im}} = q_{\mathrm{IL}} + q_{\mathrm{IG}} \tag{3}$$

where q_{IG} and q_{IL} are the gas and liquid volume inflow rates per unit perforation depth and can be described as

$$q_{\mathrm{IG}} = A_{\mathrm{I}}V_{\mathrm{ISG}},\ q_{\mathrm{IL}} = A_{\mathrm{I}}V_{\mathrm{ISL}} \tag{4}$$

where A_{I},V_{ISG}, and V_{ISL} are the cross-section area, superficial gas velocity, and superficial liquid velocity in each perforation, respectively.

Without considering the wellbore damaged zone, the equivalent point sinking radius r_{peq} is given by

$$r_{\mathrm{peq}} = \left\{-\frac{2}{l_{\mathrm{perf}}}\left[\ln\left(\frac{r_{\mathrm{perf}}}{l_{\mathrm{perf}}}\right) - s_{\mathrm{p}}\right]\right\}^{-1} \tag{5}$$

where s_{p} is the damaged skin of the cylindrical perforation and its crushed zone.

Because the interval between the perforations is big enough; therefore, for a given perforation i, each other perforation j has an influence of point sink flow $q_{\mathrm{Im},j}$.

The steady-state pressure p_{ij} of perforation i caused by perforation j can be written as

$$p_{ij} = \frac{\mu}{4\pi k}\frac{q_{\mathrm{Im},j}}{|z_i - z_j|} \tag{6}$$

Combining eqs 2 and 6, eq 1 can be described as

https://doi.org/10.1021/acsomega.1c00748
ACS Omega 2021, 6, 13066−13076

$$p_i = -\frac{\mu}{4\pi k}\frac{q_{\mathrm{Im},i}}{r_{\mathrm{peq}}} + \sum_{j\neq i}\frac{\mu}{4\pi k}\frac{q_{\mathrm{Im},j}}{|z_i - z_j|} \tag{7}$$

Let $P = (p_1, p_2, ..., p_N)^T$, $Q = (q_{\mathrm{Im},1}, q_{\mathrm{Im},2}, ..., q_{\mathrm{Im},N})^T$, eq 7 has the following vector representation

$$P = AQ \tag{8}$$

where the N-order matrix A is related to perforation parameters.[32]

2.2. Pressure Gradient Model in the Wellbore. When a gas−liquid two-phase fluid flows into a wellbore through perforation, the pressure gradient in a section of the vertical wellbore is first discussed. It is assumed that the whole perforating segment of the pipeline is uniformly divided into fixed-depth units, and each unit contains only one perforation (Figure 2).

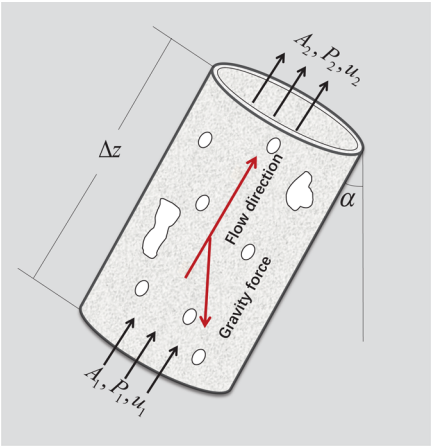

Figure 2. Diagram of the perforation unit.

The total pressure gradient in a perforation segment in a vertical wellbore consists of four different parts[32,33]

$$\Delta p_w = \Delta p_f + \Delta p_g + \Delta p_{aE} + \Delta p_{aW} \tag{9}$$

where wall friction pressure gradient is Δp_f, gravity pressure gradient is Δp_g, acceleration pressure gradient is Δp_{aE}, and Δp_{aW} which is caused by fluid expansion and wall influx, respectively.

The first term on the right-hand side of eq 9 is the pressure gradient caused by wall friction, according to the momentum balance and the mass balance

$$\Delta p_f = -\frac{\tau_w S}{A}\Delta z = -\frac{f_{tp}\rho_{tp}V_{tp}^2 S\Delta z}{2A} \tag{10}$$

where f_{tp}, V_{tp}, and ρ_{tp} are the Fanning friction factor, flow velocity, and flow density for the wellbore flow, respectively. Based on the mass balance, the total mass flow rate G_{tp} is as follows

$$G_{tp} = AV_{tp}\rho_{tp} \tag{11}$$

also

$$G_{tp} = G_L + G_G = AV_{SL}\rho_L + AV_{SG}\rho_G \tag{12}$$

where G_L and G_G are the mass flow rates of liquid and gas phases, respectively.

Combined eqs 11 and 12

$$V_{tp} = \frac{\rho_L}{\rho_{tp}}V_{SL} + \frac{\rho_G}{\rho_{tp}}V_{SG} \tag{13}$$

The second term on the right-hand side of eq 9 is the pressure gradient due to gravity

$$\Delta p_g = -g\rho_{tp}\Delta z\cos\alpha \tag{14}$$

In the homogeneous model, two-phase flow density ρ_{tp} is defined as the liquid flow and gas flow density weighted average of liquid holdup H_L

$$\rho_{tp} = \rho_L H_L + \rho_G(1 - H_L) \tag{15}$$

From engineering gas law

$$\rho_G = \frac{pM}{Z_g RT} \tag{16}$$

The ratio of the liquid flow cross-sectional area to the total cross-sectional area is referred to as a liquid fraction or liquid holdup and is defined as

$$H_L = \frac{A_L}{A} = \frac{A_L}{A_L + A_G} \tag{17}$$

where A is the wellbore's cross-sectional area and A_L and A_G are the cross-sectional areas of gas−liquid flow along the well cross section at a given depth.

The fluid holdup varies with the depth of the wellbore because the fluid density is not constant. The gas holdup is

$$H_G = \frac{A_G}{A} = 1 - H_L \tag{18}$$

The third term on the right-hand side of eq 9 is the acceleration pressure gradient because of fluid expansion, which is the product of the total pressure gradient and the coefficient of expansion[34]

$$\Delta p_{aE} = \frac{\beta_{aE}}{1 - \beta_{aE}}[\Delta p_f + \Delta p_g + \Delta p_{aW}] \tag{19}$$

where β_{aE} is an expansion coefficient that can be expressed as

$$\beta_{aE} = \frac{\rho_{tp}V_m V_{SG}}{p} \tag{20}$$

The last term on the right-hand side of eq 9 is the acceleration pressure gradient due to the wall influx. According to the mass balance and the momentum balance, the acceleration pressure gradient can be described as two forms

$$\begin{cases} \Delta p_{aW1} = -\dfrac{1}{A}\rho_{tp}\Delta z(V_m Q_{Itp} + V_{tp}Q_{Im}) \\ \Delta p_{aW2} = -\dfrac{2}{A}\rho_{tp}\Delta z V_{tp}Q_{Itp} \end{cases} \tag{21}$$

where V_m is the mixture velocity and Q_{Itp} and Q_{Im} are the two-phase and the mixture volumetric influx rate per unit wellbore depth, or

$$Q_{Itp} = \frac{\rho_L}{\rho_{tp}}Q_{IL} + \frac{\rho_G}{\rho_{tp}}Q_{IG} \tag{22}$$

$$Q_{Im} = Q_{IL} + Q_{IG} \neq Q_{Itp} \tag{23}$$

https://doi.org/10.1021/acsomega.1c00748
ACS Omega 2021, 6, 13066−13076

$$V_m = V_{SL} + V_{SG} = \frac{G_L}{A\rho_L} + \frac{G_G}{A\rho_G} \tag{24}$$

where Q_{IG} and Q_{IL} are the gas and liquid volumetric inflow rates of the unit well depth.

By matching the predictions with the experimental data, a weighted average for Δp_{aW1} and Δp_{aW2} is found to obtain the best prediction for the acceleration pressure gradient

$$\Delta p_{aW} = \omega \Delta p_{aW1} + (1 - \omega)\Delta p_{aW2} \tag{25}$$

or

$$\Delta p_{aW} = -\frac{\rho_{tp}\Delta z}{A}[\omega(V_m Q_{Itp} + U_{tp}V_{Im}) + 2(1 - \omega)V_{tp}Q_{Itp}] \tag{26}$$

Along the perforation section, the pressure $p_{w,i}$ of the perforation unit i can be presented as

$$\begin{cases} p_{w,1} = p_d \\ p_{w,i+1} = p_{w,i} + \Delta p_{f,i} + \Delta p_{g,i} + \Delta p_{aE,i} + \Delta p_{aW,i} \end{cases} \tag{27}$$

where p_d is the downstream pressure at position x_1.

In iterative eq 27, the pressure gradient $\Delta p_{f,i}$ of unit i can be estimated by

$$\Delta p_{f,i} = -\frac{S f_{tp}\rho_{tp}V_{tp}^2}{2A}|z_{i+1} - z_i| \tag{28}$$

The gravity pressure gradient $\Delta p_{g,i}$ can be evaluated as

$$\Delta p_{g,i} = -g\rho_{tp}|z_{i+1} - z_i|\cos\alpha \tag{29}$$

where α_i is the inclination angle of the perforation unit i.

The acceleration pressure gradient $\Delta p_{aE,i}$ is due to the momentum change in the wellbore when more fluid enters the wellbore through the perforations

$$\Delta p_{aE,i} = \frac{\beta_{aE}}{1 - \beta_{aE}}[\Delta p_{f,i} + \Delta p_{g,i} + \Delta p_{aW,i}] \tag{30}$$

The acceleration pressure gradient $\Delta p_{aW,i}$ because of the wall influx can be obtained as

$$\Delta p_{aW,i} = -\frac{\rho_{tp}}{A}[\omega(V_{m,i}Q_{Itp,i} + U_{tp,i}V_{Im,i}) + 2(1 - \omega) V_{tp,i}Q_{Itp,i}]|z_{i+1} - z_i| \tag{31}$$

For gas−liquid two-phase flow in the perforation area, the cumulative flow rate per wellbore depth is

$$Q_{IG,i} = \sum_{j=1}^{i-1} q_{IG,j} \tag{32}$$

$$Q_{IL,i} = \sum_{j=1}^{i-1} q_{IL,j} \tag{33}$$

2.3. Liquid Holdup Behavior. In a two-phase flow, the proportion of the pipe occupied by the one phase is often different from that of the total volumetric flow, and the gas phase moves faster than the liquid phase in an upward flow.[35,36] This is known as the holdup phenomenon, where the in situ volume fraction of the liquid phase is greater than the input volume fraction of the liquid phase.

In order to calculate the slip between the gas phase and liquid phase in the homogeneous model, the drift flux model developed by Zuber, Findlay, and Wallis was used to describe the multiphase flow in the wellbore.[37,38] The basic idea of the drift-flux model is to assume that the gas−liquid two-phase mixture is a single fluid phase, and there is slip between the two phases due to the nonuniform velocity distribution. Using an empirical constitutive relation, the velocity V_G of the gas can be related to the mixture velocity V_m

$$V_G = C_0 V_m + V_d \tag{34}$$

where C_0 is the two-phase flow distribution coefficient, which relates the average velocity to the maximum velocity of the velocity profile.[39] In a steady-state model, C_0 generally varies from 1.0 to 1.2.

In eq 34, V_d is the gas drift velocity that describes the rising velocity of the bubble relative to the average liquid velocity[9]

$$V_d = \frac{(1 - C_0 H_G)C_0 V_c K_u}{C_0 H_G\sqrt{\rho_G/\rho_L} + 1 - C_0 H_G} \tag{35}$$

where V_c is the bubble rise velocity in the liquid volume

$$V_c = \left[\frac{g\sigma_{GL}(\rho_L - \rho_G)}{\rho_L^2}\right]^{1/4} \tag{36}$$

where σ_{GL} is the surface tension between the gas phase and the liquid phase. Parameter Ku is the Kutateladze number given by Richter[9,40]

$$Ku = \left[\frac{C_{ku}}{\sqrt{N_B}}\left(\sqrt{1 + \frac{N_B}{C_{ku}^2 C_w}} - 1\right)\right]^{1/2} \tag{37}$$

where C_w is a wall friction factor and C_{ku} is a constant, which are defaulted to 0.008 and 142. Also, N_B is the Bond number defined as

$$N_B = \frac{g(\rho_L - \rho_G)D^2}{\sigma_{GL}} \tag{38}$$

According to eq 35, the gas fraction H_G and the liquid holdup H_L can be described as

$$\begin{cases} H_G = \dfrac{V_{SG}}{C_0 V_m + V_d} \\ H_L = 1 - H_G \end{cases} \tag{39}$$

2.4. Optimization Models. Perforation parameters, such as depth, density, phase angle, and so forth, affect the productivity of gas wells. This paper mainly investigates how to optimize perforation parameters according to the actual situation of the formation, considering the influence of various factors, to maximize gas wells' productivity.

Given a H_p depth vertical perforation segment, these are N perforations with coordinate z_i $(1 \le i \le N)$, which are unknown variables. Based on eq 8, the total production of the gas well can be written as[30]

$$f(z) = \sum_{i=1}^{N} [A^{-1}(z_i)P]_i \tag{40}$$

Ignoring water or gas coning in the following optimization problem. For the infinite conductivity well, the pressure gradient

https://doi.org/10.1021/acsomega.1c00748
ACS Omega 2021, 6, 13066−13076

Table 1. Parameters of the Wellbore and Reservoir Flow

parameter	value	unit	parameter	value	unit
well depth	7100	m	reservoir permeability	3.4484	10−3 μm2
perforation radius	0.01	m	perforated interval	500	m
perforation depth	0.50	m	perforation segment	25	
flow viscosity	0.55	MPa·s	crushed zone thickness	0.01	m
well diameter	0.125	m	wellbore roughness	0.001	m

Table 2. Parameters of Azimuth, Inclination, and Depth

number	measured depth (m)	inclination (deg)	Azimuth (deg)	vertical depth (m)	number	measured depth (m)	inclination (deg)	Azimuth (deg)	vertical depth (m)
1	0	0	120.33	0	13	3605	2.05	123.25	3603.36
2	303	1.97	121.2	302.87	14	3901	0.16	121.45	3899.22
3	600	1.93	120.28	599.73	15	4183	2.92	121.24	4181.09
4	899	0.75	126.57	898.59	16	4492	2.73	129.22	4489.95
5	1206	1.25	124.9	1205.45	17	4816.07	1.98	121.61	4813.87
6	1505	1.04	124.62	1504.32	18	5099.07	2.74	129.93	5096.74
7	1800	0.49	123.75	1799.18	19	5394.07	0.13	120.46	5391.61
8	2105	2.49	125.27	2104.04	20	5706.07	0.63	129.59	5703.47
9	2401	1.27	123.13	2399.91	21	5983.07	2.09	120.14	5980.34
10	2669	2.44	120.12	2667.79	22	6302.07	2.69	122.91	6299.19
11	3021	0.14	127.39	3019.63	23	6597.07	2.45	129.41	6594.06
12	3299	1.18	122.6	3297.5	24	6911.12	0.15	124.88	6907.96

relative to drawdown p_d could be negligible along with the wellbore, that is, $p_i = p_d$ $(i = 1, 2, ..., N)$, the optimization production model is obtained

$$\max f(z) = \sum_{i=1}^{N} [A^{-1}(z_i)P]_i$$

$$\text{s. t.} \begin{cases} p_i - p_d = 0, & (i = 1, 2, ..., N) \\ z_{i+1} - z_i \geq 0, & (i = 1, 2, ..., N-1) \\ z_1 \geq 0, \\ H_p - z_N \geq 0 \end{cases} \tag{41}$$

In the case of the finite conductivity well, the pressure gradient is evaluated on each perforation units, that is, $p_i = p_{wi}$. Thus, the optimized production model is determined

$$\max f(z) = \sum_{i=1}^{N} [A^{-1}(z_i)P]_i$$

$$\text{s. t.} \begin{cases} p_i - p_{wi} = 0, & (i = 1, 2, ..., N) \\ z_{i+1} - z_i \geq 0, & (i = 1, 2, ..., N-1) \\ z_1 \geq 0, \\ H_p - z_N \geq 0 \end{cases} \tag{42}$$

Above eqs 41 and 42 are two nonlinear programming problems (NLPs) with equality constraints and inequality constraints. Landman and Goldthorpe discussed various kinds of perforation distribution strategies in detail and proposed a quasi-Newton method for solving NLPs.[23]

3. RESULTS AND DISCUSSION

3.1. Simulation Parameters. A gas−liquid vertical well is studied which perforated 500 m, and a drawdown of 39.8949

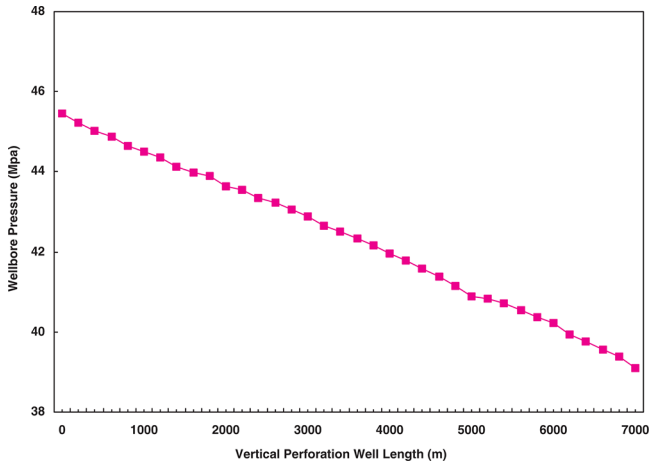

Figure 3. Pressure distribution of the wellbore.

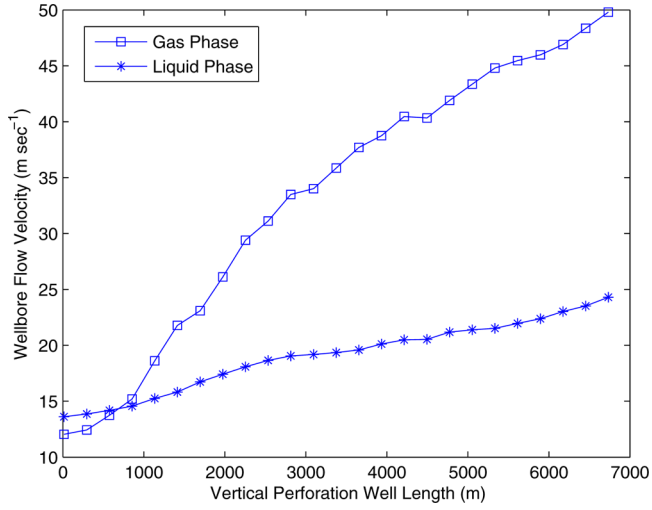

Figure 4. Velocity distribution of the wellbore flow.

https://doi.org/10.1021/acsomega.1c00748
ACS Omega 2021, 6, 13066−13076

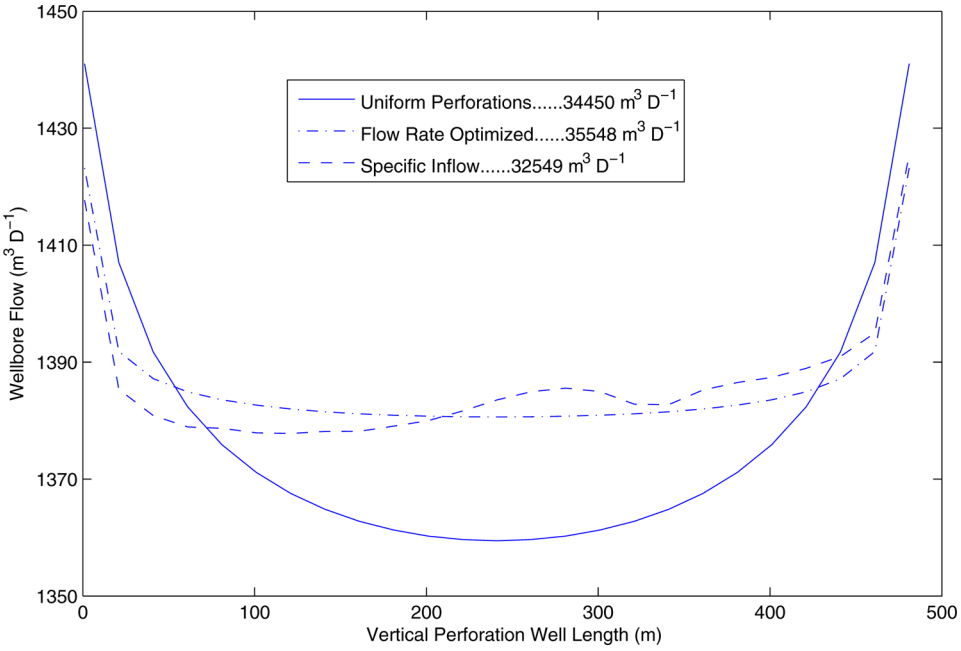

Figure 5. Inflow of the optimization model for the infinite conductivity well.

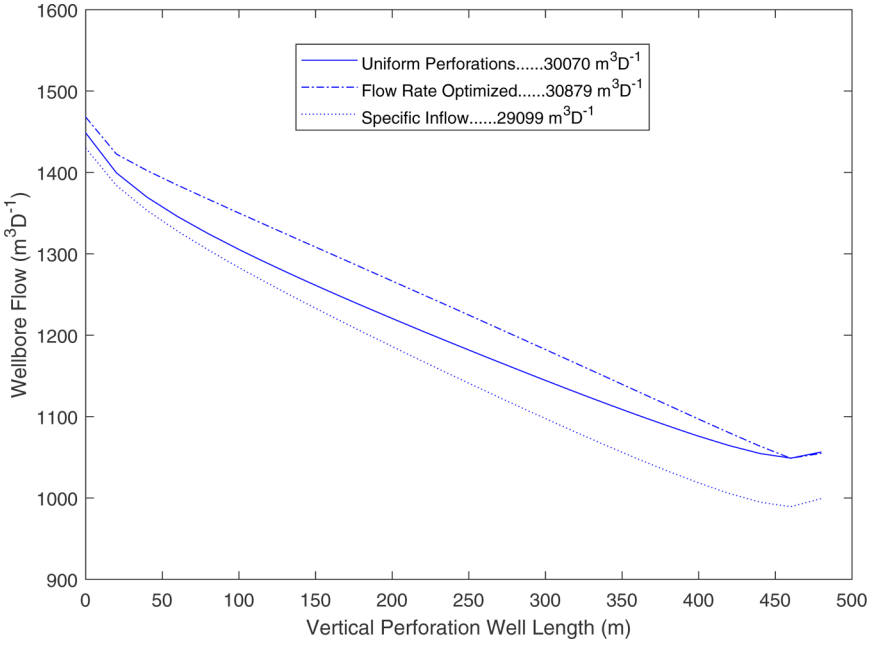

Figure 6. Inflow of the optimization model for the finite conductivity well.

MPa. More detailed parameters are shown in Tables 1 and 2, respectively.[30]

3.2. Trend Analysis. From the point of view of numerical simulation, the above model is run under the given parameters: drawdown was 39.8949 MPa, with a uniform perforation density of 5 holes per meter. The pressure and velocity results of the wellbore fluid are illustrated in Figures 3 and 4, respectively.

Perform trend analysis to check that the proposed model is physically correct. In order to verify the established model, the gas velocity, the liquid velocity, and the pressure distribution in the wellbore were measured. The pressure distribution along the entire 7100 m depth of the wellbore is shown in Figure 3. From Figure 3, we can observe that as the vertical well depth increases from bottom to top, the pressure decreases gradually. Similarly, as shown in Figure 4, we can also see the velocity trends for the gas and liquid phases.

3.3. Optimal Vertical Perforation Distribution. Through numerical simulation, a series of results of perforation wells are obtained. The pressure gradient, the flow rate of each perforating unit, and the optimal vertical perforation distribution in the wellbore are displayed in the figures and tables.

The solutions of flow-rate optimizations and flow-specific for gas−liquid wells with infinite conductivity are shown in Figures 5 and 6, and they are compared to uniformly perforated wells.

It can be seen from the production flow coupling model that the uniform perforation production is 34,450 m^3 D^{-1} at infinite conductivity and 30,070 m^3 D^{-1} at finite conductivity.

https://doi.org/10.1021/acsomega.1c00748
ACS Omega 2021, 6, 13066−13076

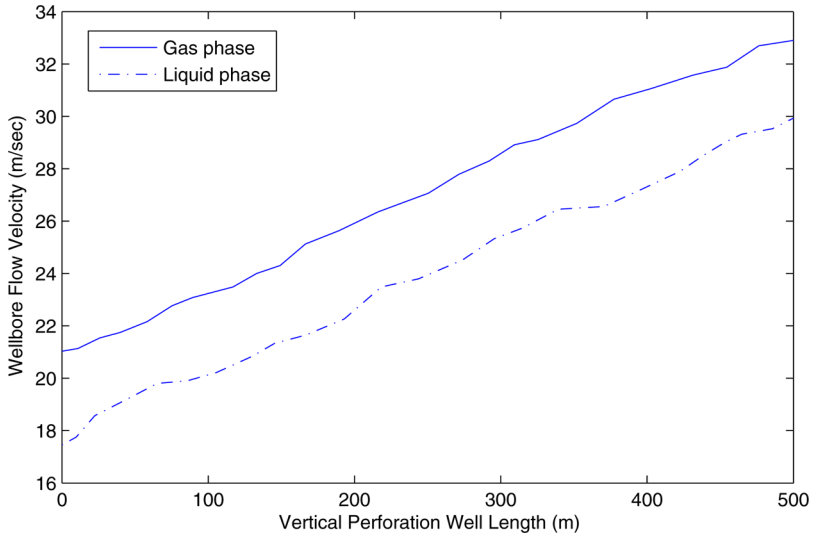

Figure 7. Velocity of the wellbore flow for the finite conductivity well.

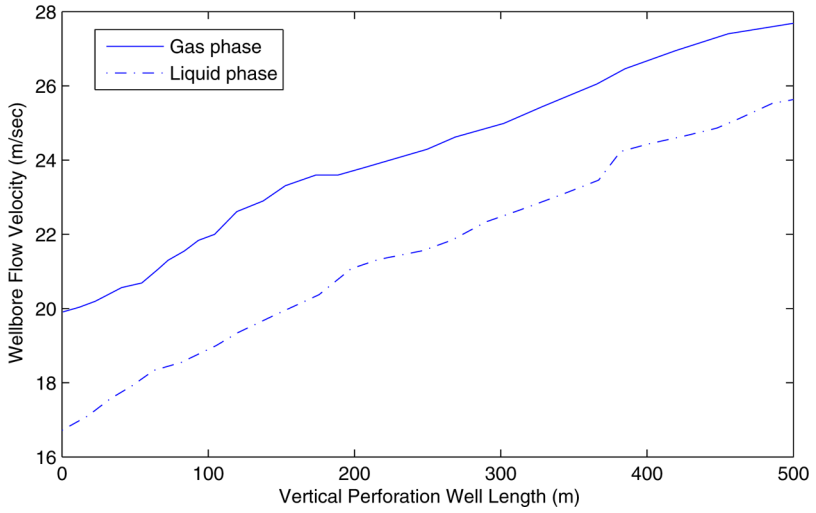

Figure 8. Velocity of the wellbore flow for the infinite conductivity well.

Figure 5 shows that the perforations are more densely distributed at the bottom and top of the perforation vertical interval. The optimal perforation productivity was 35,548 m^3 D^{-1}, an increase of 3.19% compared to a uniformly perforated well. The specific inflow seems to have little effect on the productivity, which was 32,549 m^3 D^{-1}, a 5.52% decrease compared to the uniformly perforated well.

Figure 6 shows the results for optimizing production and for making the specific inflow finitely conductive. The pressure gradient of each perforation unit was calculated. The optimal model shows that the perforations are more densely distributed in the higher inflow section. The optimal perforation productivity was 30,879 m^3 D^{-1}, which was 2.69% higher than that of the uniformly perforated well. The specific inflow has the opposite effect on the perforation distribution and has a negative effect on productivity. The productivity was 29,099 m^3 D^{-1}, which is 3.23% lower than that of the uniformly perforated well.

Figures 7 and 8 show the wellbore flow velocity of gas−liquid wells with finite conductivity and infinite conductivity, respectively. With the increment of perforations and perforating influx accumulation, wellbore flow velocity increases along with the depth of the vertical wells. Figure 9 shows the liquid holdup variation with the depth of the perforated well, ranging from 0.6823 to 0.7114. In two-phase flow, the liquid holdup is mainly determined by gas velocity and flow distribution coefficient C_0. With the increase of the gas velocity and flow distribution coefficient, liquid holdup increases.

Optimal perforation distribution is illustrated in Figures 10 and 11. Due to the large fluid supply range, a large amount of the reservoir flowed into the wellbore at the bottom and top of the perforated vertical well. The central supply range of the perforated vertical well is relatively small, so the inflow from the reservoir is small. Because there is no pressure gradient in the wellbore of an infinite conductivity well, the inflow is almost symmetrical and thus, the perforation density is symmetrically distributed. For a finite conductivity well with specific uniform inflow, the perforation density should be increased at low inflow points and decreased at high inflow points. Under a specific uniform inflow condition, the infinite conductivity well has a lower perforation flow rate and a higher density at both ends of the perforating well. Compared with the infinite conductivity well, due to the existence of the pressure gradient, the finite conductivity well has a higher inflow and a greater bottom pressure gradient.

https://doi.org/10.1021/acsomega.1c00748
ACS Omega 2021, 6, 13066−13076

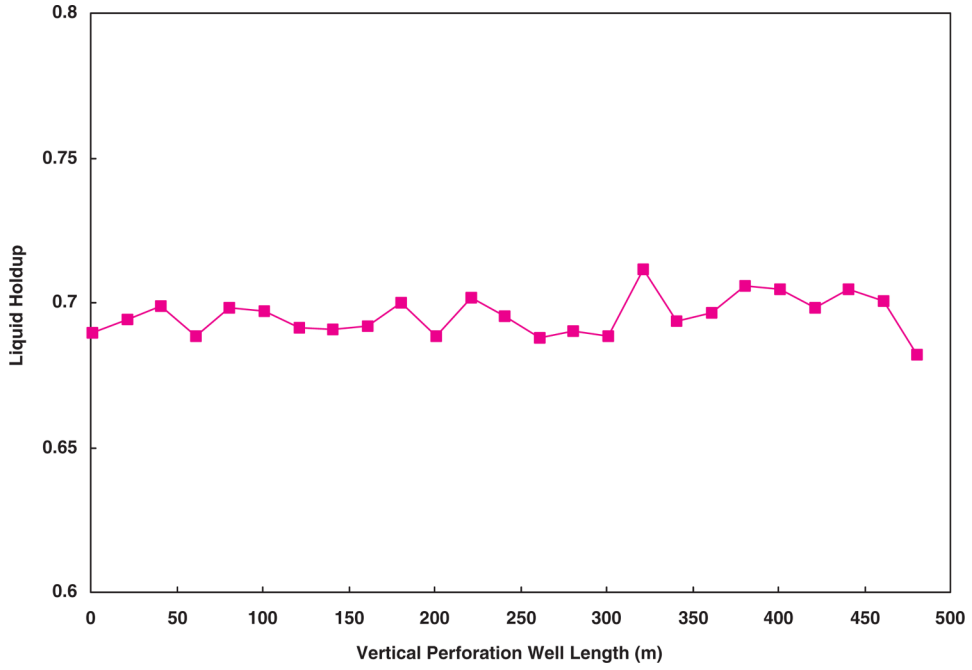

Figure 9. Liquid holdup for the optimization model of the infinite conductivity well.

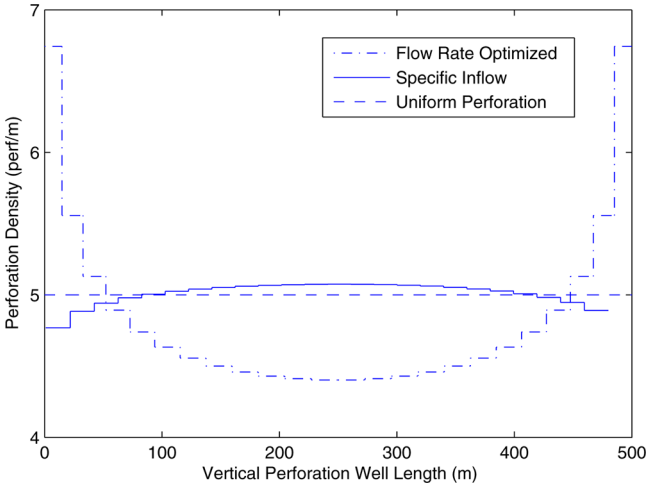

Figure 10. Optimal perforation distribution for the infinite conductivity well.

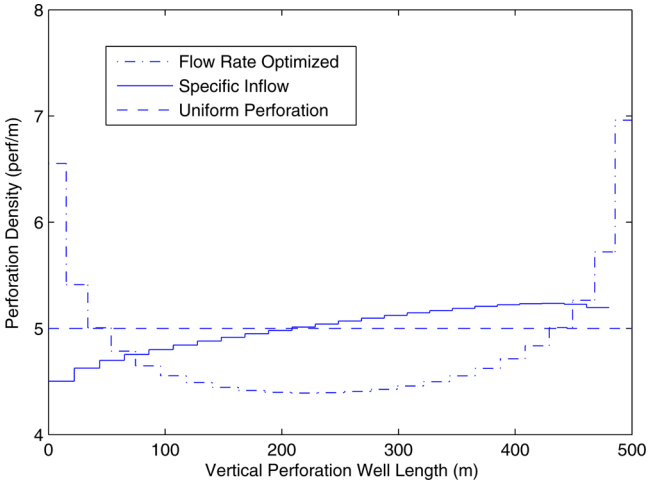

Figure 11. Optimal perforation distribution for the finite conductivity well.

3.4. Comparison Analysis. In the comparison step, the same well is used as a sample and applied to the three-phase pipeline flow proposed by Xu et al.[9] As can be seen from Figure 12, the predicted pressure and velocity performance are consistent with our models.

3.5. Sensitivity Analysis. In order to study the influence of different perforation parameters on the perforation distribution, the method of different perforation radius and perforation depth is adopted. Through numerical simulation, a series of results are obtained.

3.5.1. Effect of Perforation Radius r_{perf}. Figure 13 illustrates the perforation density as a function of the perforation radius in the range of 0.008−0.020 m. The perforation density decreases while the perforation radius increases, which could be due to fact that the larger the perforation radius, the more leakage in the wellbore. There was no significant increase in productivity, with the perforation radius increasing from 0.008 to 0.020 m and the productivity increasing from 3.42 to 4.12%. Therefore, increasing the perforation aperture has little effect on improving the button hole flow performance.

3.5.2. Effect of Perforation Depth l_{perf}. Figure 14 shows the variation of perforation density with the perforation depth when the perforation radius is 0.1 m. As can be seen from the figure, from 0.4 to 2.8 m, the perforation density decreases with the increase of the perforation depth. When the perforation depth is less than the oil damage zone, the damage zone affects the perforation inflow characteristics. When the perforation depth is greater than the oil damage zone, the perforation channel between the formation and wellbore can significantly improve the formation flow characteristics with the increase of the penetration depth.

3.6. Error Analysis. In order to estimate the performance of the proposed models, statistical parameters were used to evaluate the obtained correlation.[41−45]

The average percent relative error (ARE %) is defined in eq 43.

https://doi.org/10.1021/acsomega.1c00748
ACS Omega 2021, 6, 13066−13076

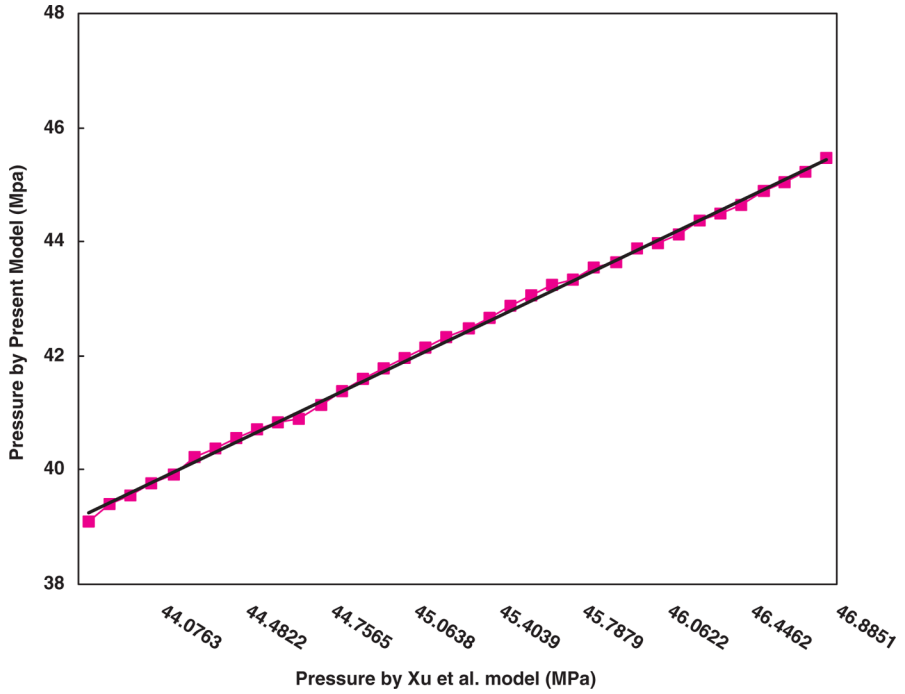

Figure 12. Comparison result of the wellbore pressure.

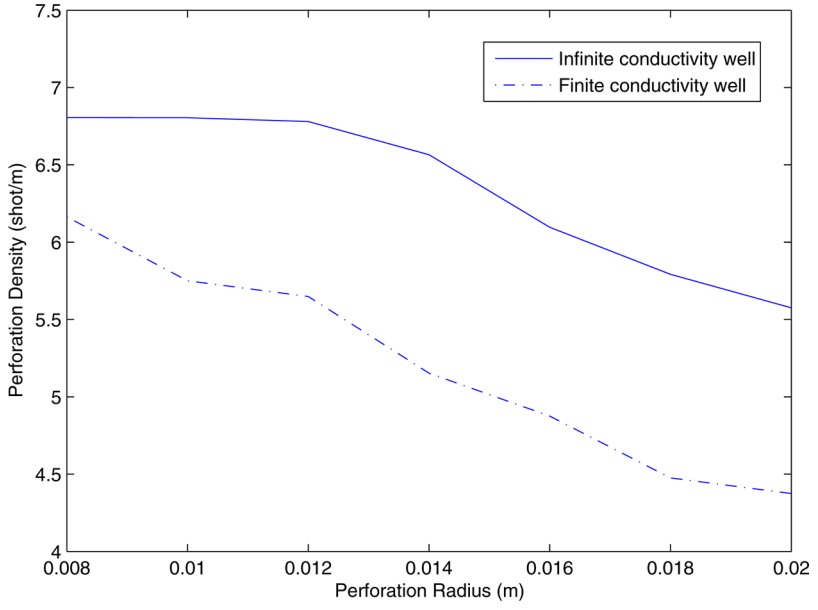

Figure 13. Influence of perforation radius on perforation density.

$$\text{ARE \%} = \frac{100}{N_d}\sum_{i=1}^{N}\left(\frac{q_i^{exp} - q_i^{calc}}{q_i^{exp}}\right) \tag{43}$$

ARE % is a measure of bias, a value of zero indicates a random distribution of the measured values around the correlation.

The arithmetic average of the absolute values of the relative errors (AARE %), an indication of accuracy, is defined in eq 44.

$$\text{AARE \%} = \frac{100}{N_d}\sum_{i=1}^{N}\left|\frac{q_i^{exp} - q_i^{calc}}{q_i^{exp}}\right| \tag{44}$$

The correlation determination R^2, a measure of the precision of the fit of the data, is defined in eq 45.

$$R^2 = 1 - \frac{\sum_{i=1}^{N_d}(q_i^{exp} - q_i^{calc})^2}{\sum_{i=1}^{N_d}(q_i^{exp} - q_{mean}^{exp})^2} \tag{45}$$

If data are perfectly correlated, then $R^2 = 1$. A small value of AARE % and an R^2 value close to 1 denote a good correlation based on good data.

Table 3 lists the statistical parameters of the currently proposed method.

In order to quantify the quality of the optimal inflow at different phasing cases, we defined the inflow error.

https://doi.org/10.1021/acsomega.1c00748
ACS Omega 2021, 6, 13066−13076

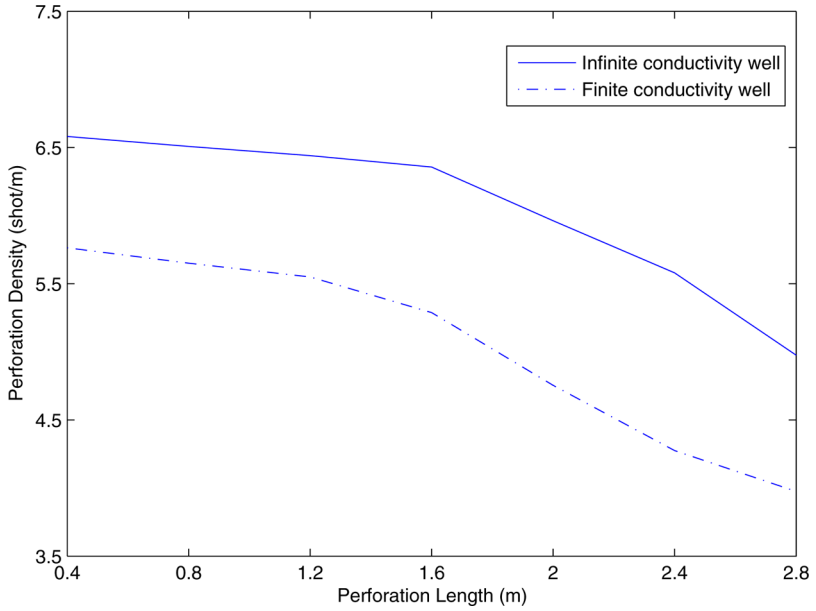

Figure 14. Effect of perforation depth on perforation density.

Table 3. Statistical Parameters of the Method Proposed in This Study

	value	
statistical parameters	infinite conductivity	finite conductivity
number of data points out of correlation	25	25
ARE %	−0.6264	−0.2127
AARE %	6.0497	6.0966
R^2	0.9834	0.9427

$$E_{qw} = \frac{1}{J}\sum_{j=1}^{J}\frac{(q_{w,j} - q_{id,j})^2}{q_{id,j}^{\ 2}} \quad (46)$$

where $q_{w,j}$, $q_{id,j}$ are the simulated inflow and the ideal inflow from the reservoir, respectively. The simulation errors of the infinite conductivity well and finite conductivity well are studied. The error E_{qw} was as defined in eq 46, the results of which are presented in Table 4.

As expected, the inflow results of inflow the optimization technology were applied. The improvement was obvious for the infinite conductivity well, such as the optimization method results in the error of the gas phase inflow from 7.313×10^{-4} to 9.310×10^{-5}.

4. CONCLUSIONS

This article describes the pressure gradient in a gas−liquid wellbore. The pressure flow coupling system model of a high-temperature and high-pressure gas−liquid two-phase well is established. A series of optimization models were established to calculate the optimal perforation distribution for a vertical wellbore. A simple application of the models in the perforated vertical well was given. Based on the basic data of the 7100 m gas−liquid well in China, a case study was carried out and the sensitivity of the model is analyzed.

Considering the influence of coning and nonconing of infinite and finite conductivity wells, the optimal perforation distribution and production of vertical perforating wells are plotted.The results showed that the model was technically reliable for HPHT gas well test designs and provided the tools for dynamic production analysis. At the same time, the model is also applicable to various types of oil and gas wells such as horizontal wells, vertical wells, and inclined wells.

More complex models of perforation inflow or multiphase wellbore pressure gradient and the effect of perforation distribution on formation fluids could be considered in the next paper.

AUTHOR INFORMATION

Corresponding Author

Jiancheng Hu − *College of Applied Mathematics, Chengdu University of Information Technology, Chengdu 610225, P. R. China*; orcid.org/0000-0002-3519-2140; Email: jianchenghu@163.com

Complete contact information is available at: https://pubs.acs.org/10.1021/acsomega.1c00748

Notes

The author declares no competing financial interest.

Table 4. Error Estimation of Wellbore Flow before and after Perforation Optimization

	before optimization			after optimization		
	total inflow	liquid phase	gas phase	total inflow	liquid phase	gas phase
infinite conductivity	1.771×10^{-3}	7.284×10^{-4}	7.313×10^{-4}	8.183×10^{-4}	8.303×10^{-5}	9.310×10^{-5}
finite conductivity	6.250×10^{-3}	6.216×10^{-4}	3.139×10^{-4}	1.024×10^{-3}	1.397×10^{-4}	9.294×10^{-5}

https://doi.org/10.1021/acsomega.1c00748
ACS Omega 2021, 6, 13066−13076

■ ACKNOWLEDGMENTS

This work was supported by the Sichuan Province Science and Technology Project (2019YFS0143).

■ REFERENCES

(1) Barnea, D. A Unified Model for Predicting Flow-Pattern Transitions for the Whole Range of Pipe Inclinations. *Int. J. Multiphase Flow* **1987**, *13*, 1−12.
(2) Xiao, J. J.; Shoham, O.; Brill, J. P. A Comprehensive Mechanistic Model for Two-Phase Flow in Pipelines. *SPE Annual Technical Conference and Exhibition*: New Orleans, LA, 1990; pp 23−25, SPE 20631.
(3) Hasan, A. R.; Kabir, C. S. Two-phase flow in vertical and inclined annuli. *Int. J. Multiphase Flow* **1992**, *18*, 279−293.
(4) Ansari, A. M.; Sylvester, N. D.; Sarica, C.; Shoham, O.; Brill, J. P. A comprehensive mechanistic model for upward two-phase flow in wellbores. *SPE Prod. Facil.* **1994**, *9*, 143−151.
(5) Petalas, N.; Aziz, K. A Mechanistic Model for Multiphase Flow in Pipes. *Proceedings, 49th Annual Technical Meeting of the Petroleum Society of the CIM*: Calgary, Alberta, Canada, 1998; pp 8−10, CIM 98-39.
(6) Kaya, A. S.; Sarica, C.; Brill, J. P. Comprehensive Mechanistic Model of Two-Phase Flow in Deviated Wells. *SPE Annual Technical Conference and Exhibition*: Houston, TX, 1999; pp 3−6, SPE 56522.
(7) Ouyang, L.-B.; Aziz, K. A Mechanistic Model for Gas-liquid Flow in Horizontal Wells with Radial Influx or Outflux. *Petrol. Sci. Technol.* **2002**, *20*, 191−222.
(8) Gomez, L. E.; Shoham, O.; Schmidt, Z.; Chokshi, R. N.; Northug, T. Unified Mechanistic Model for Steady-State Two-Phase Flow: Horizontal to Vertical Upward Flow. *SPE J.* **2000**, *5*, 339−350.
(9) Wei, N.; Xu, C.; Meng, Y.; Li, G.; Ma, X.; Liu, A. Numerical simulation of gas-liquid two-phase flow in wellbore based on drift flux model. *Appl. Math. Comput.* **2018**, *338*, 175−191.
(10) Yao, C.; Li, H.; Xue, Y.; Liu, X.; Hao, C. Investigation on the frictional pressure drop of gas liquid two-phase flows in vertical downward tubes. *Int. Commun. Heat Mass Transfer* **2018**, *91*, 138−149.
(11) Kissling, W.; McGuinness, M.; Weir, G.; White, S.; Young, R. Vertical two-phase flow in porous media. *Transp. Porous Media* **1992**, *8*, 99−131.
(12) Choi, J.; Pereyra, E.; Sarica, C.; Park, C.; Kang, J. An Efficient Drift-Flux Closure Relationship to Estimate Liquid Holdups of Gas-Liquid Two-Phase Flow in Pipes. *Energies* **2012**, *5*, 5294−5306.
(13) Yin, B. T.; Li, X. F.; Liu, G. A mechanistic model of heat transfer for gas−liquid flow in vertical wellbore annuli. *Pet. Sci.* **2018**, *15*, 135−145.
(14) Liu, Y.; Tong, T. A.; Ozbayoglu, E.; Yu, M. J.; Upchurch, E. An improved drift-flux correlation for gas-liquid two-phase flow in horizontal and vertical upward inclined wells. *J. Pet. Sci. Eng.* **2012**, *195*, 107881.
(15) Beggs, D. H.; Brill, J. P. A study of two-phase flow in inclined pipes. *J. Pet. Technol.* **1973**, *25*, 607−617.
(16) Triplett, K. A.; Ghiaasiaan, S. M.; Abdel-Khalik, S. I.; Sadowski, D. L. Gas−liquid two-phase flow in microchannels Part I: two-phase flow patterns. *Int. J. Multiphase Flow* **1999**, *25*, 377−394.
(17) Zhang, H.; Falcone, G.; Teodoriu, C. Modeling fully transient two-phase flow in the near-wellbore region during liquid loading in gas wells. *J. Nat. Gas Sci. Eng.* **2010**, *2*, 122−131.
(18) Song, X.; Guan, Z. Coupled modeling circulating temperature and pressure of gas−liquid two phase flow in deep water wells. *J. Pet. Sci. Eng.* **2012**, *92*−*93*, 124−131.
(19) Hewitt, G. F. Churn and Wispy Annular Flow Regimes in Vertical Gas-Liquid Flows. *Energy Fuels* **2012**, *26*, 4067−4077.
(20) Gao, Y.; Cui, Y.; Xu, B.; Sun, B.; Zhao, X.; Li, H.; Chen, L. Two phase flow heat transfer analysis at different flow patterns in the wellbore. *Appl. Therm. Eng.* **2017**, *117*, 544−552.
(21) Kawahara, A. Gas-Liquid Two-Phase Flows in Micro-Channels. *Int. J. Multiphase Flow* **2017**, *31*, 257−266.
(22) Islam, M. R.; Chakma, A. Comprehensive Physical and Numerical Modeling of a Horizontal Well. *SPE Annual Technical Conference and Exhibition*: New Orleans, Louisiana, September, 1990, SPE-20627-MS.
(23) Landman, M. J.; Goldthorpe, W. H. Optimization of Perforation Distribution for Horizontal Wells. *SPE Asia-Pacific Conference*: Perth, Australia, 4−7 November, 1991; pp 567−576, SPE 23005.
(24) Marett, B. P.; Landman, M. J. Optimization of Perforation Distribution for Horizontal Wells in Reservoirs with Boundaries. *SPE Asia Pacific Oil & Gas Conference & Exhibition*: Singapore, 8−10 February, 1993; pp 397−406, SPE 25366.
(25) Johns, R. T.; Lake, L. W.; Ansari, R. Z.; Delliste, A. M. Prediction of Capillary Fluid Interfaces During Gas or Water Coning in Vertical Wells. *SPE J.* **2005**, *10*, 440−448.
(26) Clemo, T. Flow in Perforated Pipes: A Comparison of Models and Experiments. *SPE Prod. Oper.* **2006**, *21*, 302−311.
(27) Hagoort, J. An analytical model for predicting the productivity of perforated wells. *J. Pet. Sci. Eng.* **2007**, *56*, 199−218.
(28) Yildiz, T. Productivity of Selectively Perforated Vertical Wells. *SPE J.* **2002**, *7*, 158−169.
(29) Wang, Z.; Wei, J.; Zhang, J.; Gong, B.; Yan, H. Optimization of perforation distribution for horizontal wells based on genetic algorithms. *Pet. Sci.* **2010**, *7*, 232−238.
(30) Xu, J.; Hu, J.; Luo, M.; Wang, S.; Qi, B.; Qiao, Z. Optimisation of perforation distribution in HTHP vertical wells. *Can. J. Chem. Eng.* **2013**, *91*, 332−343.
(31) Hu, J. Coupled Gas−Liquid Two-Phase Model in Perforated Vertical Wells for Petroleum and Natural Gas. *Energy Technol.* **2015**, *3*, 1018−1025.
(32) Hu, J.; Xu, J.; Wang, S.; Qi, B.; Qiao, Z. An optimal model for predicting the productivity of perforated vertical HTHP wells. *Can. J. Chem. Eng.* **2014**, *92*, 1247−1259.
(33) Ouyang, L.-B.; Aziz, K. A homogeneous model for gas−liquid flow in horizontal wells. *J. Pet. Sci. Eng.* **2000**, *27*, 119−128.
(34) Govier, G. W.; Aziz, K. *The Flow of Complex Mixtures in Pipes*; Van Nostrand Reinhood Comp.: New York−London, 1972.
(35) Luo, C.; Zhang, L.; Liu, Y.; Zhao, Y.; Wu, Y. An improved model to predict liquid holdup in vertical gas wells. *J. Pet. Sci. Eng.* **2019**, *184*, 106491.
(36) Ballesteros, M.; Ratkovich, N.; Pereyra, E. Analysis and Modelling of Liquid Holdup in Low Liquid Loading Two-Phase Flow Using CFD and Experimental Data. *J. Energy Resour. Technol.* **2020**, *143*, 012105.
(37) Zuber, N.; Findlay, J. A. Average volumetric concentration in two-phase flow systems. *J. Heat Transfer* **1965**, *87*, 453−468.
(38) Wallis, G. B. *One-Dimensional Two-phase Flow*; McGraw-Hill Book Comp.: New York, 1969.
(39) Taitel, Y.; Barnea, D. Two-Phase Slug Flow. *Adv. Heat Transfer* **1990**, *20*, 83−132.
(40) Richter, H. J. Flooding in Tubes and Annuli. *Int. J. Multiphase Flow* **1981**, *7*, 647−658.
(41) Jarrahian, A.; Aghel, B.; Heidaryan, E. On the viscosity of natural gas. *Fuel* **2015**, *150*, 609−618.
(42) Jarrahian, A.; Heidaryan, E. A new cubic equation of state for sweet and sour natural gases even when composition is unknown. *Fuel* **2014**, *134*, 333−342.
(43) Jarrahian, A.; Heidaryan, E. A simple correlation to estimate natural gas thermal conductivity. *J. Nat. Gas Sci. Eng.* **2014**, *18*, 446−450.
(44) Jarrahian, A.; Moghadasi, J.; Heidaryan, E. Empirical estimating of black oils bubblepoint (saturation) pressure. *J. Pet. Sci. Eng.* **2015**, *126*, 69−77.
(45) Heidaryan, E. A. Note on Model Selection Based on the Percentage of Accuracy-Precision. *J. Energy Resour. Technol.* **2019**, *141*, 045501.

https://doi.org/10.1021/acsomega.1c00748
ACS Omega 2021, 6, 13066−13076